Aggravation of Cardiac Myofibroblast Arrhythmogeneicity by Mechanical Stress

Teddy Grand, PhD,[1] Nicolò Salvarani, PhD,[1] Florian Jousset, PhD, Stephan Rohr, MD

[1]: *contributed equally to this study*

Department of Physiology, University of Bern, Bühlplatz 5, CH-3012 Bern, Switzerland

Corresponding author:

Stephan Rohr, MD
Department of Physiology
University of Bern
Bühlplatz 5
CH-3012 Bern
Switzerland

FAX: +41 31 631 46 11
Phone: +41 31 631 87 46
e-mail: rohr@pyl.unibe.ch

Abstract

Aims Myofibroblasts as appearing in the myocardium during fibrotic remodeling induce slow conduction following heterocellular gap junctional coupling to cardiomyocytes in bioengineered tissue preparations kept under isometric conditions. In this study, we investigated the hypothesis that strain developed during diastolic filling of the heart chambers may modulate myofibroblast-dependent slow conduction.

Methods and Results Effects of defined levels of strain on single cell electrophysiology (patch clamp) and impulse conduction in patterned growth cell strands (optical mapping) were investigated in neonatal rat ventricular cell cultures (Wistar) grown on flexible substrates. While 10.5% strain only minimally affected conduction times in control cardiomyocyte strands (+3.2%, n.s.), it caused a significant slowing of conduction in the fibrosis model consisting of cardiomyocyte strands coated with myofibroblasts (conduction times +26.3%). Increased sensitivity to strain of the fibrosis model was due to activation of mechanosensitive channels (MSCs) in both cardiomyocytes and myofibroblasts that aggravated the myofibroblast-dependent baseline depolarization of cardiomyocytes. As found in non-strained preparations, baseline depolarization of cardiomyocytes was partly due to the presence of constitutively active MSCs in coupled myofibroblasts. Constitutive activity of MSCs was not dependent on the contractile state of myofibroblasts because neither stimulation (thrombin) nor suppression (blebbistatin) thereof significantly affected conduction velocities in the non-strained fibrosis model.

Conclusions The findings demonstrate that both constitutive and strain-induced activity of mechanosensitive channels in myofibroblasts significantly enhance their depolarizing effect on electrotonically coupled cardiomyocytes. Ensuing aggravation of slow conduction may contribute to the precipitation of strain-related arrhythmias in fibrotically remodeled hearts.

Keywords: Arrhythmia, slow conduction, fibrosis, myofibroblast, strain

1. Introduction

Old age, genetic predisposition and insults to the heart like mechanical overload and infarction are well established causes of fibrotic remodeling of the working myocardium.[1] Remodeled tissue is characterized by the presence of excess amounts of collagen that compromises mechanical pump function and promotes arrhythmogenesis by disruption of the normally uniform electrical substrate for impulse propagation.[2] Excess secretion of extracellular matrix (ECM) proteins is primarily attributed to 'activated' fibroblasts (myofibroblasts, MFBs) that appear in the working myocardium of diseased hearts.[3] Apart from contributing to structural tissue remodeling, MFBs have been shown to exert direct arrhythmogenic effects on cardiomyocytes (CMCs) following establishment of heterocellular gap junctional coupling based on connexin 43 (Cx43) and connexin 45 (Cx45) in cell culture systems.[4] In the presence of heterocellular gap junctional coupling, experiments showed that depolarizing current flow from moderately polarized MFBs to well polarized CMCs causes the latter to undergo partial depolarization thereby inducing slow conduction, precipitation of ectopic activity and initiation of reentrant arrhythmias.[5-7]

In contrast to cell cultures grown on rigid substrates that undergo isometric contractions, intact cardiac tissue exhibits phasic length changes during the pump cycle with maximal strain present in end-diastole. With few exceptions, it has generally been found that stretching healthy cardiac tissue within physiological limits (from slack length to length of maximal tension development) causes a proportional increase in conduction velocities (θ) when measured in observer coordinates (θ_{observ} as obtained, e.g., from optical recordings) while conduction times between two specific reference points within the stretched tissue (CT_{prep}) remain largely unchanged (for detailed review cf.[8]). While these findings are normally discussed in the framework of CMC stretch sensitivity, work by Kamkin and colleagues suggested that cardiac fibroblasts may be involved in the response of the myocardium to stretch as well. They reported that mechanical stress causes changes in fibroblast polarization due to activation of mechanosensitive channels (MSCs) that may, if electrotonically coupled to CMCs, may affect the electrophysiology of the latter.[9] Similarly, Kohl and colleagues have shown in a model that strain-induced fibroblast depolarization may affect the discharge rate of electrotonically coupled sinoatrial pacemaker cells thereby contributing to the adaptation of the heart rate to atrial filling pressure.[10]

Given these findings, the question arises to which extent MFBs may modulate conduction velocities in diseased fibrotic myocardia subjected to stretch and relaxation. Because a direct investigation of this question in intact tissue exhibiting a complex cellular composition and architecture is not feasible with presently available methodologies, we developed an in-vitro cell culture system with controlled geometry and defined cellular composition that permits the direct assessment of the differential contribution of CMCs and MFBs to changes of θ during application of defined levels of stretch and relaxation. Using this model, we investigated the hypotheses that (i) immunocytochemically defined cardiac myofibroblasts respond to stretch with a reduction of membrane polarization, that (ii) stretch

induced depolarization of MFBs aggravates slow conduction in strands of electrotonically coupled cardiomyocytes, and that (iii) mechanical strain exerted by contractile MFBs on adjacent cardiomyocytes may directly affect propagation. Our findings show that physiological levels of longitudinal fiber strain as observed in intact healthy tissue during diastolic filling (< 10%)[11] have no significant effects on CT_{prep} in preparations consisting predominantly of CMCs. In the presence of electrotonically coupled MFBs, however, CT_{prep} increases proportionally to applied stretch suggesting that MFBs act as potent sensors of mechanical stress that cause substantial slowing of conduction in electrotonically coupled CMCs. Such MFB-mediated sensitization of fibrotic cardiac tissue to strain may contribute to the mechanistic understanding of arrhythmogenesis in fibrotically remodeled hearts subject to mechanical stress.

2. Methods

2.1 Cell culture model

Experiments were conducted in agreement with relevant institutional and Swiss Federal guidelines for animal experimentation. Primary cultures of 1-day old Wistar neonatal rat ventricular CMCs and MFBs were established using previously published methods.[12] Animals were decapitated, hearts removed and the ventricular tissue was dissociated with trypsin. The resulting cell suspension containing CMCs and non-CMCs was subjected to differential pre-plating in order to separate fast adhering fibroblasts (dominating cell type of non-CMC fraction) from slowly adhering CMCs. Adherent fibroblasts underwent a phenotype switch to MFBs within 1-2 days and were used in experiments after 8 days.

Single cell cultures: For patch clamp experiments, CMCs or MFBs were seeded at 40 to 500 cells/mm^2 on collagen (Type I or IV, Sigma) coated glass coverslips or on silicone membranes. Before cell seeding, silicone membranes (Silastic, SMI, USA) were mounted on a digital caliper and pre-stretched by ~ 20%. A cell culture well was produced by glueing a silicone ring (28/2 mm; Semadeni, Switzerland) to the membrane with silicone adhesive. Experiments were performed on 3 to 4 day old preparations.

Patterned growth cultures: For optical recording of impulse propagation under non-strained conditions, CMCs were seeded at a density of 1500 cells/mm^2 on photolithographically pretreated coverslips that were designed to produce uniform cell strands measuring 0.6 x 5 mm.[12] For strain experiments, lines of collagen were applied with a fine point nib (500 to 900 µm wide) to the bottom of the flexible culture wells. Hybrid CMC-MFB cell strands were obtained by coating 24 h old CMC strand preparations with MFBs at a density of 500 cells/mm^2 which resulted in a CMC to MFB ratio of 3:1. Experiments were performed on 3 to 4 day old preparations.

2.2 Optical measurement of impulse conduction

Impulse propagation along strand preparations was assessed optically using the voltage sensitive dye di-8-ANEPPS (Biotium). Experiments were conducted at 36°C and signals were recorded after pre-stimulation of the preparations for 10 s at 2 Hz. Recordings were made with a 20x objective (spatial resolution: 50 µm). Signals acquired at 20 kHz were digitally filtered prior to analysis (f_o: 0.5 kHz). Optically recorded action potential amplitudes were normalized (%APA) and maximal upstroke velocities (dV/dt_{max}) were calculated in units of %APA/ms. For the case of an action potential amplitude of 100 mV, values given in units of %APA/ms are identical to values in units of V/s.

2.3 Patch-clamp recording

Cell electrophysiology of CMCs and MFBs was assessed using standard whole-cell patch clamp techniques (HEKA EPC-10). Signals were filtered (1 kHz), digitized (2.9 kHz) and stored for off-line analysis. The pipette filling solution contained (in mmol/L): K-aspartate 120, NaCl 10, MgATP 3, $CaCl_2$ 1, EGTA 10, Hepes 5 (pH 7.2). Pipette resistances ranged from 4 to 6 MΩ. Series resistance and, after rupturing of the patch, cell capacitance were compensated and voltage values were corrected for liquid junction potentials (-12.4 mV). I-V relationships of CMCs and MFBs were obtained with voltage ramp protocols. Whole cell currents were normalized to cell capacitance and are reported as pA/pF. For stretch/relaxation experiments, recordings were obtained within 25 min after application of defined levels of strain.

2.4 Wrinkle experiments

Substrates for the wrinkle assay (Excellness, Switzerland) were coated with collagen type IV, sterilized with UV and coated with MFBs at low density (100 cells/mm^2). During experiments, preparations were continuously superfused at 36°C with Hank's balanced salt solution (HBSS) containing 1% neonatal calf serum (NCS). Time lapse video recordings served to assess the changes of wrinkle patterns following drug addition. Custom-made software (MatLab; The MathWorks, Natick, MA) was used to quantify the time course of the change in the wrinkle area during experiments.

2.5 Immunocytochemistry

Presence of myofibroblasts was confirmed by staining the preparations for α-smooth muscle actin and counterstaining the nuclei with DAPI using standard protocols.

2.6 Solutions

In all experiments, preparations were superfused at 2-3 ml/min with HBSS containing 1% neonatal calf serum and 10 mmol/L Hepes (pH 7.40). For gadolinium experiments, a solution devoid of phosphate and bicarbonate was used that contained (in mmol/L): NaCl 140, KCl 5.4, $CaCl_2$ 1.8, $MgCl_2$ 1.2, Glucose 20, Hepes 5 (pH 7.40). Drugs used were obtained from Sigma, except thrombin (Biopur AG, Switzerland).

2.7 Statistics

Values are given as mean ± SD in the text and in the bar graphs. Number of samples refer to independent experiments. Data were compared using a 2-tailed Student *t* test (homoscedastic or heteroscedastic where appropriate) and differences between data sets were considered significant at $p<0.05$.

A detailed description of the methods used can be found in the Online Supplement.

3. Results

3.1 Validation of the experimental model

The effects of stretch and relaxation on action potential propagation were investigated in tissue engineered cell strands grown on silicone membranes that were fixed to the arms of a sliding digital caliper (Figure 1A). During experiments, the entire assembly was placed on the stage of an inverted microscope, the preparation was superfused at 36°C and cell strands under investigation were stimulated with an extracellular electrode (Figure 1B). A typical example of optically recorded action potential upstrokes during propagated activity along a non-strained cardiomyocyte cell strand is shown in Figure 1C. Experimental preparations consisted either of cardiomyocytes (CMC cell strands exhibiting a low degree of 'contamination' with MFBs; Figure 2Aa) or of CMC cell strands uniformly coated with myofibroblasts (CMC-MFB cell strands; Figure 2Ab). Important in the context of patch clamp experiments, fibroblasts seeded on silicone membranes displayed a rapid phenotype switch to MFBs as shown by abundant expression of α-smooth muscle actin containing stress fibers after 2 days in culture (Figure 2Ac). As shown in Figure 2B in a time series of images recorded with a high resolution camera (2048 x 2048 pixels, Ximea), strand preparations retained their stretched morphology beyond the maximal duration of the experiments. Being initially stretched by 5.5%, the example shown relaxes only slightly by 0.3% during 31 min of maintained stretch. As summarized in Figure 2C, this behavior was typical for all four types of preparations used in this study, i.e., preparations retained their stretched geometry during prolonged application of static stretch (CMC strands: 0.01 ± 0.31%, n=16; CMC-MFB strands: -0.07± 0.29%, n=22; single cell CMC preparations: -0.21±0.70%, n=21; single cell MFB preparations: 0.26±0.80%, n=10; no significant differences among different types preparations). Optical determinations of the dependence of conduction velocity on strain in CMC and CMC-MFB strands consisted of initial control measurements followed by recordings during constant application of 5% relaxation or 5% stretch, respectively. This was followed by control recordings after returning to initial conditions. Preparations were included in the analysis only if measurements obtained after returning to initial lengths were not statistically different from initial control recordings.

3.2 Effects of acute length changes on impulse conduction velocities and conduction times in cell strands

Conduction velocities in observer coordinates (θ_{observ}) were assessed at control lengths and immediately after stretching and relaxing the silicone membranes by 5% each (overall length change of 10.5%). As shown in Figure 3A, changing the overall length of CMC cell strands by 10.5 % caused θ_{observ} to increase significantly by 7.1% from 325.7±26.4 mm/s to 348.8±39.9 mm/s (n=25, $p<0.05$). With 335.8±27.8 mm/s, θ_{observ} recorded under non-strained control conditions fell exactly between θ_{observ} measured during relaxation and stretch, respectively. Maximal upstroke velocities (dV/dt_{max}) of propagating action potentials in CMC cell strands were not significantly affected by either manoeuver (control: 71.4±3.0 %APA/ms; 5% stretch: 71.6±5.0 %APA/ms; 5% relaxation: 71.5±4.0 %APA/ms; n=25, n.s.). A completely opposite behavior was observed in CMC-MFB cell strands where 5% stretch caused a slowing of θ_{observ} from 276.7±44.2 mm/s to 255.0±46.6 mm/s ($p<0.05$) whereas relaxation by 5% tended to increase θ_{observ} to 291.4±48.7 mm/s (n.s.). Considering the overall effect, stretching CMC-MFB preparations by 10.5% induced a highly significant decrease of θ_{observ} by -12.5% ($p<0.005$, n=25). Maximal upstroke velocities were not significantly affected by the different strain conditions (control: 45.9±13.4 %APA/ms; 5% stretch: 45.6±13.4 %APA/ms; 5% relaxation: 47.6±11.3 %APA/ms; n=20, n.s.).

Because preparations underwent defined levels of stretch and relaxation, changes of conduction times in preparation coordinates (CT_{prep}) during stretch and relaxation relative to control can be inferred by normalizing $\theta_{observ,\ intervention}$ to $\theta_{observ,\ control}$ followed by multiplication of the results with the length changes applied (0.95 for relaxation; 1.05 for stretch). The respective data shown in Figure 3B demonstrate that conduction times in CMC cell strands were not significantly affected by an overall lengthening of 10.5%. By contrast, the same amount of strain caused a highly significant increase of CT_{prep} in CMC-MFB cell strands (+26.3%; $p < 0.0001$).

3.3 Strain-induced mechanosensitive currents in myofibroblasts and cardiomyocytes

To investigate whether modulation of conduction by strain is based on changes in resting polarization of CMCs and/or MFBs secondary to activation of MSCs, we assessed to which extent basic electrophysiological characteristics of the two cell types are affected by stretch. For this purpose, cells were grown at low densities on silicon membranes and were subjected to whole cell patch clamp recordings either under non-strained conditions or immediately after stretching the substrate by 5% (for detailed clamp protocols cf. Data Supplement). In accordance with the protocols used for optical experiments, patch clamp recordings were limited to 25 min following onset of static stretch. Mean I-V relationships obtained from MFBs under control conditions (n=13) and during application of 5% stretch (n=8) are shown in Figures 4Aa and 4Ab with Figure 4Ac showing the superposition of the two I-V relationships. As can be gathered from the difference between the two relationships (Figure 4Ad), 5% stretch induced an outward rectifying current that reversed polarity at -12.8 mV. At -65

mV, a potential typically observed in CMC coupled to MFB,[13] stretch nearly doubled the inward current present under control conditions from -0.20±0.11 pA/pF to -0.36±0.3 pA/pF. Neither cell capacitance (125.7±67.9 pF vs. 125.3±74.5 pF) nor input resistance (1.5±0.6 GΩ vs. 1.1±0.6 GΩ) of MFBs were significantly affected by stretch. The same type of experiments conducted with CMCs yielded, as illustrated by the stretch-induced difference current in Figure 4Bd (difference between the mean I-V relationships of 12 control and 13 stretched cells), a more complex response with no consistent stretch-induced changes at potentials positive to -50 mV. Below this value, 5% stretch induced an inward current that reached a maximum at -76 mV (-0.2 pA/pF) before declining again and turning into an outward current at potentials negative to – 88 mV. Cell capacitance of CMCs was not significantly affected by stretch (18.4±6.6 pF vs. 17.6±9.6 pF) whereas their input resistance increased from 1.0±0.5 GΩ to 2.4±0.7 GΩ ($p<0.005$). As shown in Figure 4C, strain-induced inward currents caused a significant reduction of the membrane potential of MFBs from -35.6±5.9 mV (n=13) to -26.1±3.1 mV (n=8; $p<0.001$) and CMCs from -78.0±3.2 mV (n=12) to -70.8±8.3 mV (n=13; $p< 0.05$).

3.4 Contribution of MSCs to conduction under non-strained conditions

The finding that relaxation of CMC-MFB cell strands caused a significant decrease of conduction times suggested that MSCs of MFBs were contributing to conduction also under non-strained control conditions. Accordingly, we investigated the effects of the MSC blockers streptomycin (SM, 50 µmol/L) and gadolinium (Gd^{3+}, 50 µmol/L; dissolved in appropriate low phosphate buffers)[14] on the membrane voltage of CMCs and MFBs cultured under non-strained conditions. As shown in Figure 5A, the drugs had no effect on the resting polarization of CMCs (SM: -75.4±1.3 mV vs. -75.7±1.5 mV; n=6, n.s.; Gd^{3+}: -76.1±2.9 mV vs. -76.3±2.9 mV; n=11, n.s.) indicating that MSCs of CMCs were not active under non-strained conditions. By contrast, both MSC blockers caused MFBs to undergo a significant hyperpolarization (SM: -29.4±7.8 mV to -34.3±7.4 mV; n=9, $p<0.005$; Gd^{3+}: -32.2±11.6 mV to -48.2±11.7 mV; n=9, $p<0.005$) suggesting that MSCs contribute importantly to the membrane polarization of MFBs under non-strained conditions. In accordance with these single cell data and as shown in Figure 5B, SM had no effect on θ (control: 336.3±24.4 mm/s; SM: 329.5±21.4 mm/s; n=58; n.s.) and dV/dt_{max} (control: 75.2±6.1%APA/ms; SM: 75.2±5.3 %APA/ms; n=58; n.s.) in non-strained CMC cell strands. By contrast, SM caused a significant increase of both θ (173.8±68.2 mm/s to 224.9±63.3 mm/s; n=54; $p<0.005$) and dV/dt_{max} (29.8±13.3 %APA/ms to 38.5±14.3 %APA/ms; n=54; $p<0.005$) in CMC-MFB cell strands. Because Gd^{3+} was substantially more effective in hyperpolarizing MFBs than SM, this compound was expected to surpass the effect of SM in increasing θ in CMC-MFB strands. However, both CMC and CMC-MFB strands consistently showed conduction blocks in the presence of Gd^{3+} which is likely explained by its capacity to cause significant depression of sodium and calcium inward currents in cardiomyocytes.[15, 16] Overall, the results demonstrate that MFBs exhibit basal MSC activity under non-strained conditions that adds to

their depolarized phenotype and, accordingly, contributes to slow conduction in CMC-MFB cell strands also under non-strained control conditions.

3.5 Effects of acute changes of the contractile state of MFBs on their membrane potential

Tension development is a characteristic feature of myofibroblasts and, in the heart, is well established to be responsible for infarct scar consolidation.[17] The finding of basal MSC activity in non-strained MFBs raises the question of whether tension exerted by contractile MFBs on their substrate may feed back onto their own cell membrane in a manner that causes auto-activation of MSCs. This hypothesis was investigated by exposing MFBs to a blocker (blebbistatin) and an activator (thrombin) of MFB contractility.[18] The extent and time course of change of tension development by MFBs following addition of these drugs was assessed using a wrinkle assay where the extent of deformation of the extracellular substrate (wrinkle formation) is a qualitative measure of tension exerted by adherent cells on the substrate.[19] In the example shown in Figure 6A, a single MFB caused extensive wrinkles in the substrate under control conditions. Following addition of 10 µmol/L blebbistatin to the superfusate, the area occupied by wrinkles declined by ~ 50% within 10 min which reflects the drug-induced decrease of tension exerted by the MFB on their substrate (cf. also corresponding time lapse movie in the Online Data Supplement). Overall and as shown in Figure 6B, exposure of MFBs to 10 µmol/L blebbistatin for 20 min caused a significant reduction of the wrinkle area by 30.3±23.7% ($n=9$, $p<0.005$). Vice versa, exposure to 1 U/ml thrombin caused the wrinkle area to increase by 75.2±43.1% ($n=10$; $p<0.005$) which reflects a substantial increase of tension developed by MFBs. Time courses of the decrease (blebbistatin) and increase (thrombin) of the wrinkle area are shown in Figure 1 of the Data Supplement. Determination of the resting polarization of MFBs exposed for a similar time to identical concentrations of the drugs demonstrated that blebbistatin had no significant effect on the membrane potential (control: -31.6±11.2 mV; blebbistatin: -34.2±11.8 mV; $n=9$, n.s.) whereas thrombin, contrary to the hypothesis, caused a hyperpolarization despite increasing the tension developed by MFBs (control: 31.0±6.4 mV; thrombin: -34.2±9.2 mV; $n=9$, $p<0.05$). These findings suggest that MFB contractility does not directly contribute to basal activity of MSCs in non-strained preparations by auto-activation of these channels.

3.6 Effects of modulation of MFB contractility on impulse propagation in hybrid cell-strands

For hybrid cell strands consisting of MFBs cultured on top of CMCs, mechanical tension developed by MFBs is likely to be transmitted by adhesion junctions to underlying CMCs. Ensuing forces acting on the cell membrane of CMCs may modulate conduction by activation of MSCs in CMCs.[20] Accordingly, increasing (thrombin) or decreasing (blebbistatin) tension developed by MFBs attached to CMCs is expected to slow and accelerate conduction, respectively. As shown in Figure 7A,

exposure of CMC cell strands to 10 µmol/L blebbistatin for ≥ 20 min caused a slight reduction of θ from 375.7±35.6 mm/s to 365.3±42.9 mm/s (n=47; $p<0.05$) that was accompanied by an equally slight decrease of dV/dt_{max} from 78.8±5.6 %APA/ms to 76.7±10.1 %APA/ms (n=47; $p<0.05$). In CMC-MFB cell strands, blebbistatin had no effects on θ (control: 230.6±34.8 mm/s; blebbistatin: 225.2±35.1 mm/s; n=55; n.s.) and dV/dt_{max} (control: 52.2±10.4 %APA/ms; blebbistatin: 51.8±7.8 %APA/ms; n=55; n.s.). As shown in Figure 7B, exposure of CMC cell strands to thrombin at 1 U/ml for ≥ 20 min had no effects on θ (control: 352.7±34.2 mm/s; thrombin 348.2±44.1 mm/s; n=45; n.s.) and dV/dt_{max} (control: 74.8±8.5 %APA/ms; thrombin 73.4±10.9 %APA/ms; n=45; n.s.). Similarly, in CMC-MFB strands, thrombin did neither affect θ (control: 246.6±53.8 mm/s; thrombin 258.6±45.9 mm/s; n=47; n.s.) nor dV/dt_{max} (control: 45.8±14.4 %APA/ms; thrombin: 49.8±11.9 %APA/ms; n=47; n.s.) The finding that neither blebbistatin nor thrombin affected conduction in hybrid cell strands suggests that tension exerted by MFBs on adjacent CMCs is not sufficient to modulate MSC activity of CMCs to an extent large enough to affect impulse conduction in hybrid CMC-MFB preparations.

4. Discussion

The results of this study demonstrate that impulse conduction in bioengineered strands of cardiomyocytes responds to moderate levels of relaxation and stretch highly similar to intact tissue, i.e., conduction times remain largely unchanged for physiological length changes as those encountered in end-diastole where maximal strain along the direction of the fibers amounts to ~ 10%.[11] By contrast, in the presence of myofibroblasts simulating a fibrotically remodeled myocardium, impulse propagation is rendered highly sensitive to strain as reflected by a 3% increase of conduction time per each percent of lengthening. Given that the myocardium is maximally strained in end-diastole, these findings suggest that adverse electrotonic interactions between MFBs and CMCs are equally maximal at the time of electrical activation of the myocardium thereby causing aggravation of slow conduction beyond values reported before for models of the fibrotically remodeled myocardium kept under isometric conditions.

4.1 Effects of strain on conduction in cardiomyocyte preparations

Overall elongation of CMC cell strands by 10.5% caused a significant increase of optically measured conduction velocities (θ_{observ}) from 326 to 349 mm/s (+7.1%). Under the simplifying assumption that electrical membrane properties and tissue resistance remained unaffected by the moderate amount of stretch applied, simple geometrical reasoning predicts that the increase of θ should equal the amount of stretch applied. θ_{observ} was slightly slower than this predicted value (7.1% vs. 10.5%) and, accordingly, CT_{prep} showed a small increase by 3.2%. In single CMCs, 5% strain induced a significant depolarization from -78 mV to -71 mV. This result is in agreement with previous studies using intact cardiac tissue or freshly isolated adult cardiomyocytes.[21, 22] CMC depolarization was based on a

strain-induced inward current that peaked at -76 mV, i.e., close to the resting potential of non-strained cells (-78 mV). The current declined in both depolarizing and hyperpolarizing direction showing reversal potentials at -50 mV and -88 mV respectively. While no further identification of this current was undertaken in the present study, a similarly U-shaped mechanosensitive current observed in murine ventricular cardiomyocyte was shown to be due to stretch-dependent inactivation of I_{K1} which would explain the observation that strain significantly increased the input resistance of CMCs.[23, 24] Assuming that CMCs forming the cell strands underwent the same degree of strain-induced depolarization, the finding that it had no major effect on θ is likely explained by the circumstance that conduction in cardiac tissue is little affected by changes in resting polarization in the range of -80 mV to -70 mV because of the presence of supernormal conduction.[25-27] This is illustrated schematically in Figure 8 where the grey curve depicts the dependence of conduction velocity on the resting membrane potential of CMCs as derived from a previous study with cultured strands of CMCs.[27] Typical for supernormal conduction, θ increases with increasing CMC depolarization from ~ -85 mV to -75mV before declining rapidly with further depolarization. When inserting the resting potentials measured in this study for non-strained CMCs (~ - 78 mV) and CMCs subjected to 5% strain (~ - 71 mV) into this graph, it becomes evident that the substantial and significant depolarization of CMCs induced by 5% strain has a very limited effect on θ which is reflected by the experimental finding that conduction times remained unchanged during this intervention. Additional factors contributing to the modest dependence of θ on strain may include stretch dependent modulation of sodium currents, membrane capacity and intercellular resistance.[8, 28-30] Important for this study, the results show that conduction in bioengineered strands of neonatal CMCs behaves identical to intact cardiac tissue from adult animals, i.e., conduction remains largely unchanged during application of physiological levels of strain which suggests that this preparation is a suitable model for investigating the effects of strain on conduction at the cellular level.[8, 31, 32]

4.2 Effect of strain on conduction in the fibrosis model

In contrast to the lack of significant effects of strain on conduction in CMC cell strands, applying identical strains to hybrid CMC-MFB cell strands caused a significant increase of conduction times by 26.3%. This contrasting result suggests that MFBs 'sensitize' CMCs to strain. The combination of three basic mechanisms as summarized schematically in Figure 8 is likely to explain this observation: (i) As shown before, gap junctional coupling of moderately polarized MFBs to well polarized CMCs causes convergence of the membrane potentials of the two cell types based on electronic current flow from MFBs to CMCs.[5] The resulting depolarization of CMCs to values less negative than -70 mV pushes non-strained networks of CMCs beyond membrane potentials supporting the peak of supernormal conduction, i.e., into a range where every additional depolarization further slows conduction due to increasing levels of sodium channel inactivation (Figure 8: green dashed lines).[25] (ii) As shown in this study, such additional depolarization is produced in CMCs by activation of

MSC-dependent inward currents at potentials below -50 mV that aggravate the preexisting, MFB induced depolarized state of CMCs. (iii) Additionally, strain applied to MFBs evokes mechanosensitive inward currents at potentials less negative than -12.8 mV. The resulting depolarization of MFBs will accentuate depolarizing current flow to electrotonically coupled CMCs thereby further reducing the membrane voltage of CMCs (Figure 8: green solid lines). Overall, strain-induced activation of MSCs in both CMCs and MFBs that occur on top of the 'background' depolarization of CMCs by electrotonically coupled MFBs is likely to form the basis for the increased sensitivity of the fibrotic tissue model to strain. In analogy, strain sensitivity of conduction may also be increased in other pathologic conditions like hyperkalemia or ischemia where cardiac tissue is depolarized beyond membrane potentials supporting the peak of supernormal conduction.

4.3. Constitutive activity of MSCs in myofibroblasts

The finding that relaxation of cell strands by 5% caused a significant decrease of conduction times in hybrid CMC-MFB cell strands but not in CMC-strands suggests that the membrane polarization of MFBs but not CMCs is affected by basal activity of MSCs present under non-strained conditions. In accordance with previous findings in acutely isolated atrial fibroblasts,[9] the presence of constitutively active MSCs in myofibroblasts but not CMCs was supported by the finding that two blockers of MSCs, SM and Gd^{3+}, caused a significant hyperpolarization of MFBs but failed to affect the membrane voltage of CMCs under non-strained conditions. Consistent with the presence of basal activity of MSCs in MFBs that accentuates membrane depolarization of electrotonically coupled CMCs under non-strained conditions, superfusion of hybrid CMC-MFB cell strands with SM caused a significant increase of θ and dV/dt_{max} but had no effect on CMC cell strands. While an even larger effect was expected to occur in the presence of Gd^{3+} that caused substantial hyperpolarization of MFBs, Gd^{3+} dissolved in the low-phosphate / low-bicarbonate superfusate necessary to prevent buffering of Gd^{3+} consistently induced conduction block.[14] Induction of block was likely related to the suppression of sodium and calcium inward currents by Gd^{3+} which was reported to occur at concentrations similar to those used in the present study.[15, 16] Overall, these findings suggest that the modest membrane polarization typically recorded from MFBs kept under non-strained conditions is partly due to depolarizing inward currents carried by constitutively active MSCs. Candidates for these MSCs include TRPC6, TRPM4, TRPM7 and TRPV2 which exhibit substantial expression at the mRNA level.[13] Immunocytochemistry revealed that TRPV2 is targeted to the cell membrane of MFBs at the site of the leading lamella whereas TRPC6 shows increased expression at sites of cell-to-cell contact of neighboring MFBs (cf. Data Supplement).

4.4. Effect of myofibroblast contractility on MSC activity and conduction in the fibrosis model

Given the presence of basal activity of MSCs in non-strained myofibroblasts, the question arises as to whether this activity is due to tonic tensile forces exerted by MFBs that feed back onto their own cell membrane thereby causing 'auto-activation' of MSCs. This hypothesis was tested by assessing changes in membrane voltage of MFBs superfused with established activators (thrombin) and blockers (blebbistatin) of MFB contractility.[18] While, as shown by the wrinkle assay, both substances affected tension exerted by cardiac MFBs on their substrate according to expectations (increased tension with thrombin, reduced tension with blebbistatin), they did either not affect the membrane potential of MFBs (blebbistatin) or even caused a hyperpolarization (thrombin) which makes it unlikely that tension developed by MFBs causes auto-activation of MSCs.

Consistent with the small effects of blebbistatin and thrombin on the membrane potential of single MFBs, exposure of hybrid CMC-MFB cell strands to these drugs failed to affect θ and dV/dt_{max}. Theses findings demonstrate that modulation of MFB contractility alone is unable to affect impulse conduction in hybrid CMC-MFB preparations. This conclusion is supported by previous findings showing that communication incompetent HeLa cells, even though exerting tensile forces on their substrate similar to MFBs, fail to affect impulse propagation when seeded on top of CMC cell strands.[5, 33]

5. Study limitations

In contrast to intact cardiac tissue undergoing phasic variations of strain, methodological restrictions imposed by the technique used in this study required measurements to be performed under static strain conditions. However, given that mechanosensitive currents of CMCs from rats and humans were reported before to activate promptly with applied strain and to display virtually no time dependence,[22] effects of phasic variations of strain on impulse conduction may be indirectly deduced from the strain – θ relationship presented in this study. Further limitations of the study are related to the question as to which extent the in-vitro model reflects the situation in-vivo: whereas the model used in this study is well characterized in terms of cellular morphology, heterocellular gap junctional coupling, ion current densities and ratios of MFB-to-CMC cell membrane areas, the respective data from cells in-situ are still largely missing because their measurement is technically not yet feasible. Accordingly, while the results contribute to the understanding of biophysical mechanisms governing conduction in strained cardiac tissue consisting of electrotonically interacting CMCs and MFBs, the extent to which these mechanisms are operational in-vivo has to await the development of experimental methods suitable to investigate this question directly in intact tissue. This concerns especially the lack of unequivocal proof for the presence of heterocellular electrotonic coupling between MFBs and CMCs in the working myocardium of fibrotically remodeled hearts. [10, 34] Also, it cannot be ruled out that fibroblasts present in intact hearts may add an additional layer of complexity to the response of cardiac tissue to stretch. Finally, the model used is based on neonatal rat ventricular cells. Whereas this limits extrapolations of results to intact human cardiac tissue, the finding that

bioengineered preparations consisting predominantly of CMCs rather accurately reproduce the strain-sensitivity of intact healthy tissue from adult mammals suggests that the biophysical principles governing the dependence of θ on strain are likely similar.

6. Conclusions

Whereas impulse conduction in healthy cardiac tissue shows little dependence on physiological levels of strain, the results of this study suggest that myofibroblasts present in cardiac tissue undergoing fibrotic remodeling may convey increased strain sensitivity to the tissue with conduction velocities being inversely related to applied strain. Extrapolated to intact fibrotic tissue, this mechanism would imply that impulse conduction is slowest at the moment of electrical activation because activation coincides with the moment of maximal distension of the myocardium in end-diastole. Moreover, in diseased hearts displaying non-uniform mechanics, the mechanism may similarly increase non-uniformities of conduction. Pending verification in intact tissue, both effects would contribute to arrhythmogenesis in fibrotically remodeled myocardia.

Supplementary material

Supplementary material is available at *Cardiovascular Research* online.

Funding

The work was supported by the Swiss National Science Foundation [138297 to S.R.], by the European Network for Translational Research in AF [EUTRAF, 261057 to S.R.] and by the Leducq Foundation [to S.R.].

Acknowledgments

We wish to thank Regula Flückiger-Labrada for her excellent cell culture work, Stephan Schmutz for the development of computer algorithms to quantify wrinkle formation, Jan Kucera for constructive discussions and for providing the theoretical basis for assessing substrate deformation, and Sarah Moyle for critically reading the manuscript.

Conflict of interest

None declared.

References

1. Rohr S. Arrhythmogenic implications of fibroblast-myocyte interactions. *Circ Arrhythm Electrophysiol* 2012;**5**:442-452.
2. de Bakker JM, van Capelle FJ, Janse MJ, Tasseron S, Vermeulen JT, de Jonge N, Lahpor JR. Slow conduction in the infarcted human heart. 'Zigzag' course of activation. *Circulation* 1993;**88**:915-926.
3. Weber KT, Sun Y, Bhattacharya SK, Ahokas RA, Gerling IC. Myofibroblast-mediated mechanisms of pathological remodelling of the heart. *Nat Rev Cardiol* 2013;**10**:15-26.
4. Rohr S. Myofibroblasts in diseased hearts: new players in cardiac arrhythmias? *Heart Rhythm* 2009;**6**:848-856.
5. Miragoli M, Gaudesius G, Rohr S. Electrotonic modulation of cardiac impulse conduction by myofibroblasts. *Circ Res* 2006;**98**:801-810.
6. Miragoli M, Salvarani N, Rohr S. Myofibroblasts induce ectopic activity in cardiac tissue. *Circ Res* 2007;**101**:755-758.
7. Zlochiver S, Munoz V, Vikstrom KL, Taffet SM, Berenfeld O, Jalife J. Electrotonic myofibroblast-to-myocyte coupling increases propensity to reentrant arrhythmias in two-dimensional cardiac monolayers. *Biophys J* 2008;**95**:4469-4480.
8. McNary TG, Sohn K, Taccardi B, Sachse FB. Experimental and computational studies of strain-conduction velocity relationships in cardiac tissue. *Prog Biophys Mol Biol* 2008;**97**:383-400.
9. Kamkin A, Kiseleva I, Isenberg G. Activation and inactivation of a non-selective cation conductance by local mechanical deformation of acutely isolated cardiac fibroblasts. *Cardiovasc Res* 2003;**57**:793-803.
10. Kohl P, Kamkin AG, Kiseleva IS, Noble D. Mechanosensitive fibroblasts in the sino-atrial node region of rat heart: interaction with cardiomyocytes and possible role. *Exp Physiol* 1994;**79**:943-956.
11. Rademakers FE, Rogers WJ, Guier WH, Hutchins GM, Siu CO, Weisfeldt ML, Weiss JL, Shapiro EP. Relation of regional cross-fiber shortening to wall thickening in the intact heart. Three-dimensional strain analysis by NMR tagging. *Circulation* 1994;**89**:1174-1182.
12. Rohr S, Fluckiger-Labrada R, Kucera JP. Photolithographically defined deposition of attachment factors as a versatile method for patterning the growth of different cell types in culture. *Pflugers Arch* 2003;**446**:125-132.

13. Rosker C, Salvarani N, Schmutz S, Grand T, Rohr S. Abolishing myofibroblast arrhythmogeneicity by pharmacological ablation of alpha-smooth muscle actin containing stress fibers. *Circ Res* 2011;**109**:1120-1131.

14. Caldwell RA, Clemo HF, Baumgarten CM. Using gadolinium to identify stretch-activated channels: technical considerations. *Am J Physiol* 1998;**275**:C619-621.

15. Lacampagne A, Gannier F, Argibay J, Garnier D, Le Guennec JY. The stretch-activated ion channel blocker gadolinium also blocks L-type calcium channels in isolated ventricular myocytes of the guinea-pig. *Biochim Biophys Acta* 1994;**1191**:205-208.

16. Li GR, Baumgarten CM. Modulation of cardiac Na+ current by gadolinium, a blocker of stretch-induced arrhythmias. *Am J Physiol* 2001;**280**:H272-H279.

17. Sun Y, Weber KT. Infarct scar: a dynamic tissue. *Cardiovasc Res* 2000;**46**:250-256.

18. Wipff PJ, Rifkin DB, Meister JJ, Hinz B. Myofibroblast contraction activates latent TGF-beta1 from the extracellular matrix. *J Cell Biol* 2007;**179**:1311-1323.

19. Harris AK, Wild P, Stopak D. Silicone rubber substrata: a new wrinkle in the study of cell locomotion. *Science* 1980;**208**:177-179.

20. Thompson SA, Copeland CR, Reich DH, Tung L. Mechanical coupling between myofibroblasts and cardiomyocytes slows electric conduction in fibrotic cell monolayers. *Circulation* 2011;**123**:2083-2093.

21. Kamkin A, Kiseleva I, Wagner KD, Leiterer KP, Theres H, Scholz H, Gunther J, Lab MJ. Mechano-electric feedback in right atrium after left ventricular infarction in rats. *J Mol Cell Cardiol* 2000;**32**:465-477.

22. Kamkin A, Kiseleva I, Isenberg G. Stretch-activated currents in ventricular myocytes: amplitude and arrhythmogenic effects increase with hypertrophy. *Cardiovasc Res* 2000;**48**:409-420.

23. Dyachenko V, Husse B, Rueckschloss U, Isenberg G. Mechanical deformation of ventricular myocytes modulates both TRPC6 and Kir2.3 channels. *Cell Calcium* 2009;**45**:38-54.

24. McNary TG, Sachse FB. Modeling Effects of Strain-Modulated Membrane Capacitance and Conductance of K(+) Inward Rectifier on Conduction Velocity in Cardiac Tissue. *Cinc: 2009 36th Annual Computers in Cardiology Conference* 2009:381-384.

25. Kagiyama Y, Hill JL, Gettes LS. Interaction of acidosis and increased extracellular potassium on action potential characteristics and conduction in guinea pig ventricular muscle. *Circ Res* 1982;**51**:614-623.

26. Shaw RM, Rudy Y. Electrophysiologic effects of acute myocardial ischemia. A mechanistic investigation of action potential conduction and conduction failure. *Circ Res* 1997;**80**:124-138.

27. Rohr S, Kucera JP, Kleber AG. Slow conduction in cardiac tissue, I: effects of a reduction of excitability versus a reduction of electrical coupling on microconduction. *Circ Res* 1998;**83**:781-794.

28. Banderali U, Juranka PF, Clark RB, Giles WR, Morris CE. Impaired stretch modulation in potentially lethal cardiac sodium channel mutants. *Channels (Austin)* 2010;**4**:12-21.

29. Beyder A, Strege PR, Reyes S, Bernard CE, Terzic A, Makielski J, Ackerman MJ, Farrugia G. Ranolazine decreases mechanosensitivity of the voltage-gated sodium ion channel Na(v)1.5: a novel mechanism of drug action. *Circulation* 2012;**125**:2698-2706.

30. Mills RW, Narayan SM, McCulloch AD. Mechanisms of conduction slowing during myocardial stretch by ventricular volume loading in the rabbit. *Am J Physiol* 2008;**295**:H1270-H1278.

31. Penefsky ZJ, Hoffman BF. Effects of stretch on mechanical and electrical properties of cardiac muscle. *Am J Physiol* 1963;**204**:433-438.

32. Rosen MR, Legato MJ, Weiss RM. Developmental changes in impulse conduction in the canine heart. *Am J Physiol* 1981;**240**:H546-554.

33. Wolfenson H, Bershadsky A, Henis YI, Geiger B. Actomyosin-generated tension controls the molecular kinetics of focal adhesions. *J Cell Sci* 2011;**124**:1425-1432.

34. Camelliti P, Green CR, LeGrice I, Kohl P. Fibroblast network in rabbit sinoatrial node: structural and functional identification of homogeneous and heterogeneous cell coupling. *Circ Res* 2004;**94**:828-835.

FIGURES

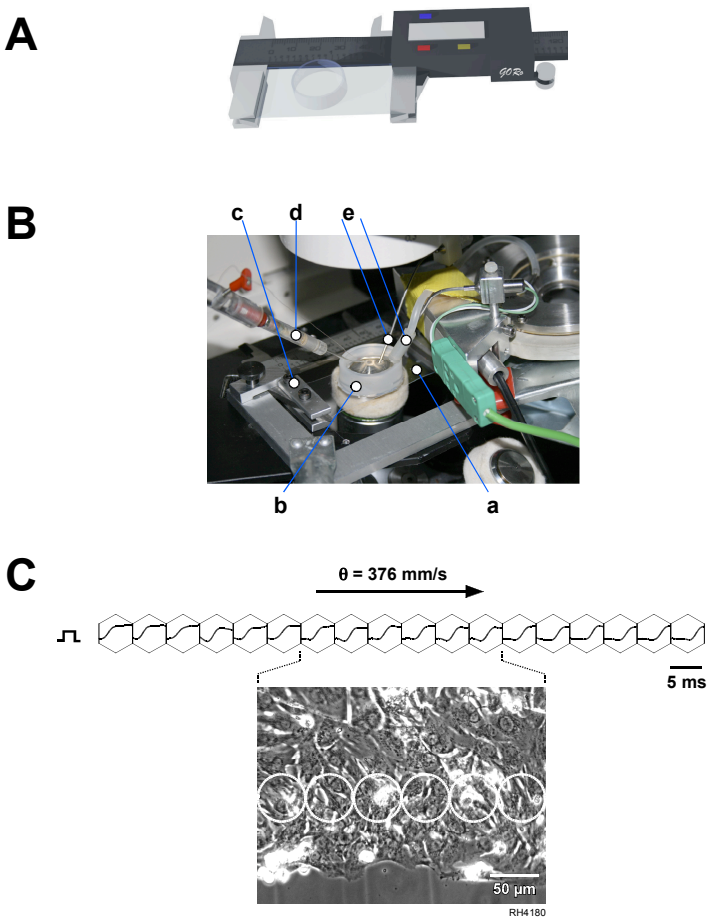

Figure 1

Figure 1 Experimental setup. **A:** Schematic drawing of the stretch device that consisted of a digital caliper whose jaws were attached to the culture 'dish' formed by a silicone ring glued to the rectangular silicone membrane. **B:** Photograph of the stretch device mounted on the stage of an inverted microscope: (a) silicone membrane, (b) silicone ring, (c) left jaw of the caliper, (d) stimulation electrode, (e) inlet/outlet of temperature-controlled superfusion system. **C:** Example of an optical control measurement of a cardiomyocyte strand preparation. Optical signals within hexagonal frames show action potential upstrokes of a propagated impulse measured by individual detectors. The morphology of the preparation is shown in the phase contrast image below with circles indicating the measurement areas of the central 6 photodetectors.

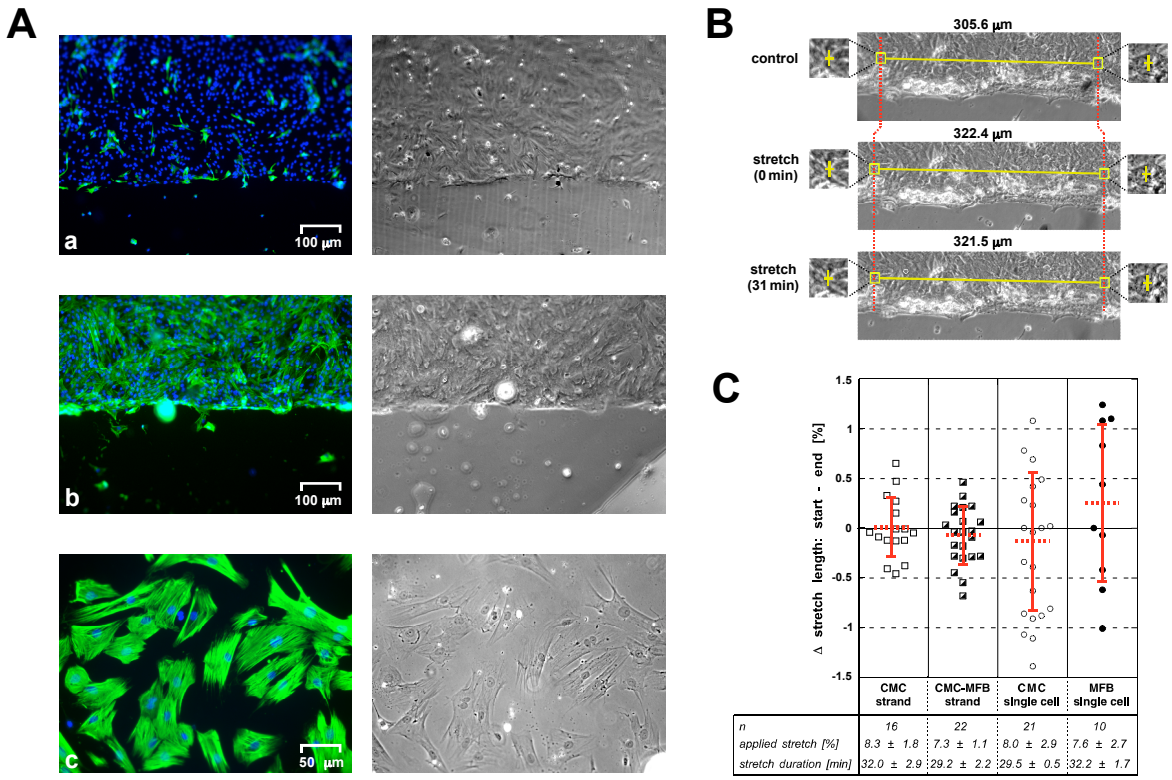

Figure 2

Figure 2 Structural characterization of preparations grown on silicone membranes and validation of the stretch procedure. **A:** Structure and cellular composition of the experimental preparations: *Aa:* Cardiomyocyte (CMC) cell strand with 'contaminating' myofibroblasts (MFBs: α-smooth muscle actin staining (green); nuclear counterstaining with DAPI (blue); corresponding phase contrast image on the right). *Ab:* Same for a hybrid CMC-MFB cell strand. *Ac:* Same for single cell MFB preparation as used in patch clamp experiments. **B:** Phase contrast images of the border region of a CMC strand before stretch (control), immediately after application of stretch, and at the end of a 31 min period of maintained stretch. Enlarged regions on both sides of the images depict the reference points within the preparation that were used for distance measurements. **C:** Changes of the lengths of the four different types of experimental preparations (CMC cell strands, CMC-MFB cell strands, CMC single cell cultures, MFB single cell cultures) along the main strain axis during stretch maintained for the duration and magnitude indicated.

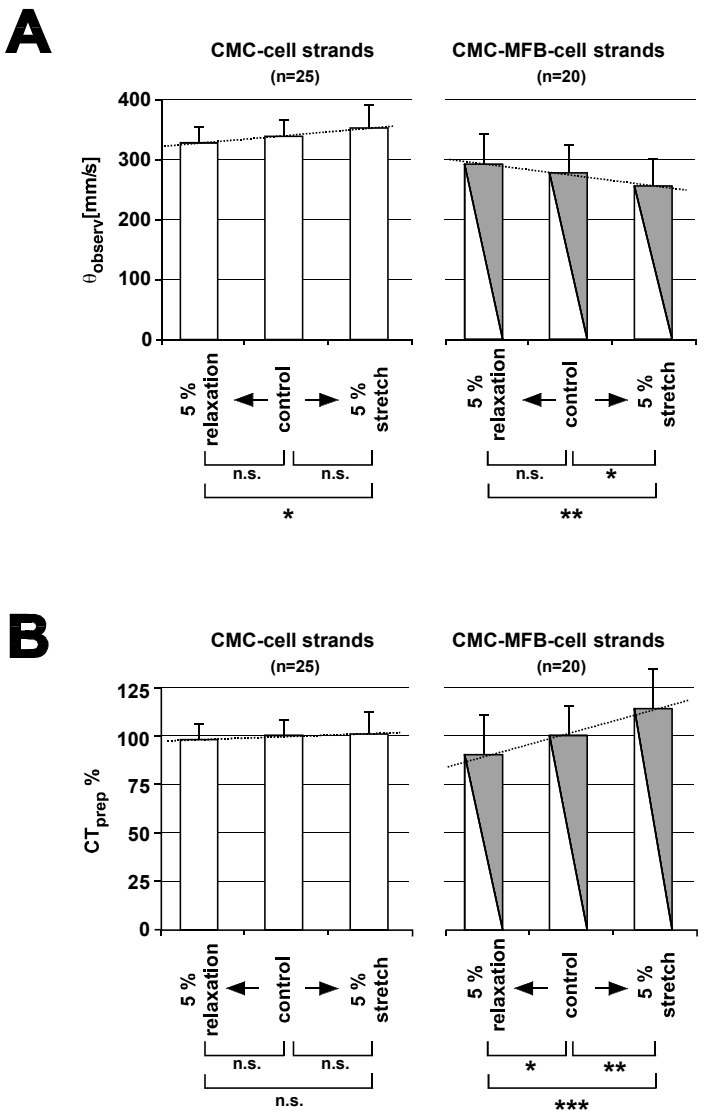

Figure 3

Figure 3 Effects of acute length changes of cell strands on conduction velocity and conduction times. **A:** Impulse conduction velocity measured optically (θ_{observ}) along strands of cardiomyocytes (CMC strands, left panel) and hybrid cardiomyocyte-myofibroblast strands (CMC-MFB strands, right panel) during shortening ('relaxation') and extension ('stretch') of the preparations by 5% each. **B:** Effects of stretch and relaxation on conduction times (CT_{prep}) of CMC cell strands (left panel) and hybrid CMC-MFB cell strands (right panel). Data are normalized to CT_{prep} obtained under control conditions. *: $p < 0.05$; **: $p < 0.005$; ***: $p < 0.0005$.

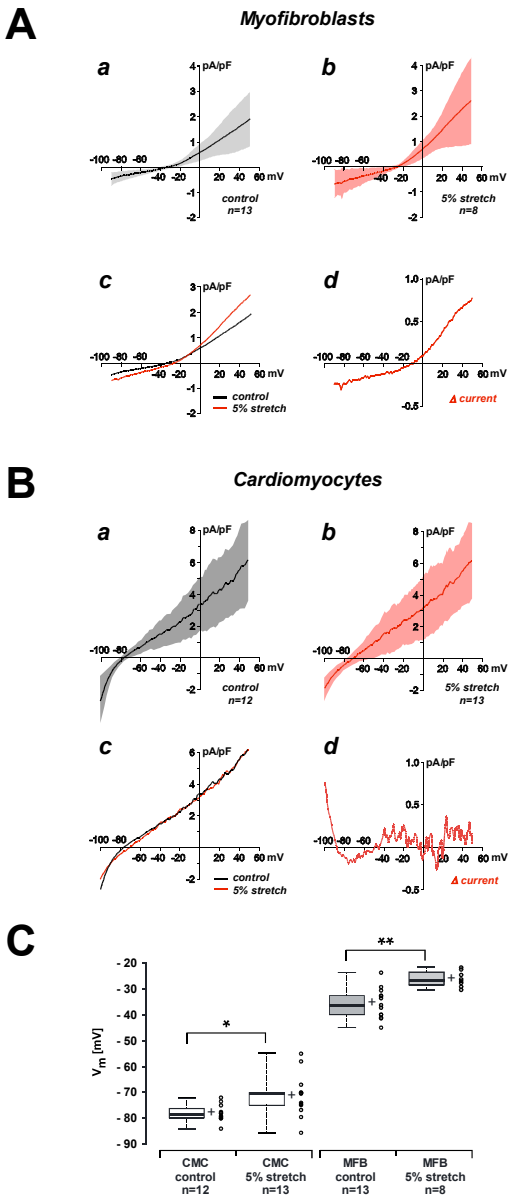

Figure 4

Figure 4 Effects of 5% stretch on single cell electrophysiology of cardiomyocytes and myofibroblasts. **A:** Mean I-V relationships of myofibroblasts obtained with ramp protocols under control conditions (Aa: mean ± SD; SD shown as band) and during application of 5% stretch (Ab). Ac: Superposition of mean I-V curves obtained under control conditions (black) and during application of 5% stretch (red). Ad: Mean difference current induced by 5% stretch. **B:** Same as A for cardiomyocytes. **C:** Change of resting polarization of cardiomyocytes (CMCs) and myofibroblasts (MFBs) in response to application of 5% stretch. *: $p < 0.05$; **: $p < 0.005$.

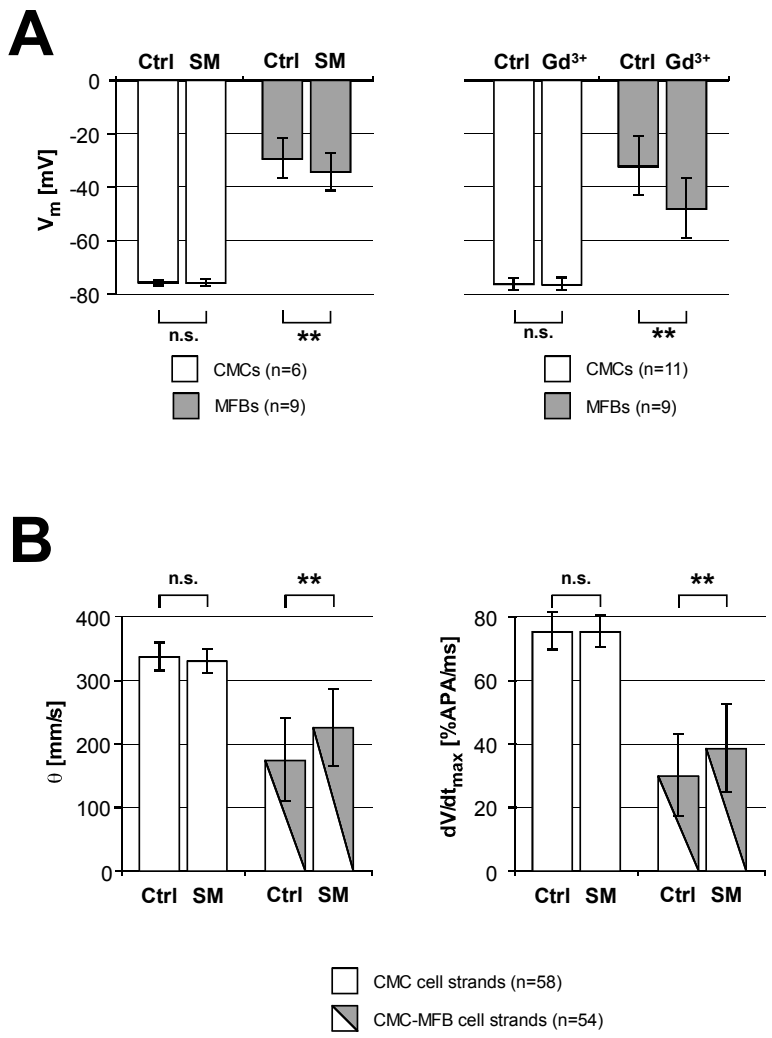

Figure 5

Figure 5 Effects of blocking mechanosensitive channels on resting polarization and impulse propagation. **A:** Change of resting polarization of cardiomyocytes (CMCs) and myofibroblasts (MFBs) during exposure to streptomycin (SM; left panel) and gadolinium (Gd^{3+}; right panel). **B:** Effect of SM on conduction velocity (θ; left panel) and maximal upstroke velocities (dV/dt_{max}; right panel) of propagated action potentials in CMC and CMC-MFB cell strands. **: $p < 0.005$.

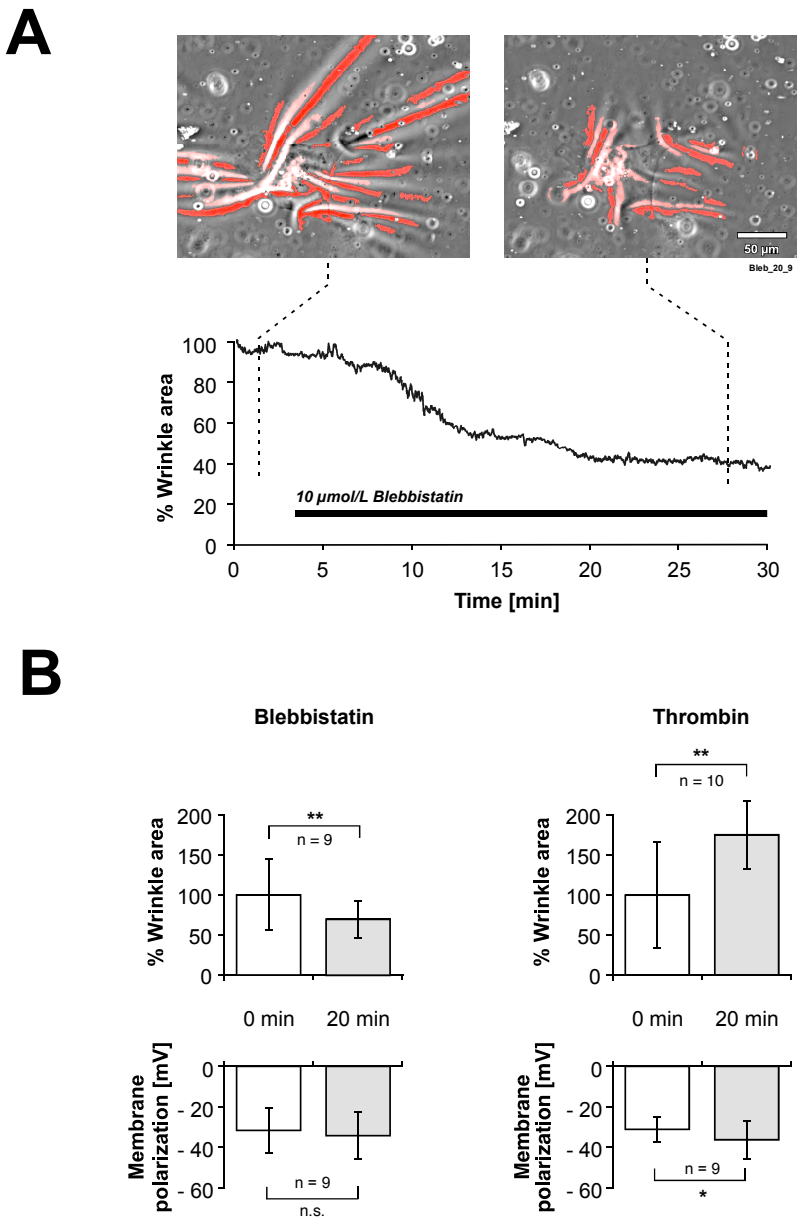

Figure 6

Figure 6 Modulation of myofibroblast tension development by blebbistatin and thrombin. **A:** Phase contrast images of wrinkle patterns before and after exposure of the preparation to blebbistatin (10 µmol/L). The panel below illustrates the time course of the reduction of the area occupied by wrinkles. **B:** Effects of blebbistatin (left panels) and thrombin (right panels) on wrinkle formation and membrane potential of cardiac myofibroblasts.

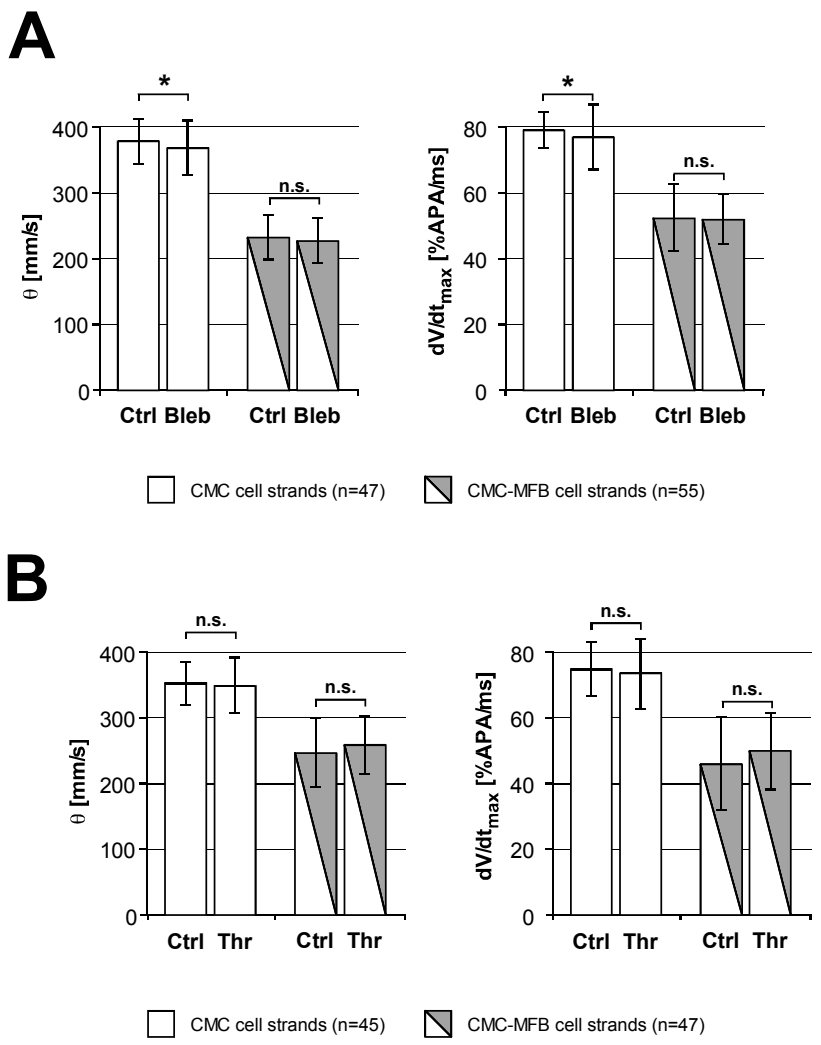

Figure 7

Figure 7 Effects of modulators of myofibroblast contractility on impulse propagation in strand preparations. **A:** Effects of reducing MFB contractility with blebbistatin on θ (left panel) and dV/dt_{max} (right panel) in CMC and CMC-MFB cell strands. **B:** Effects of increasing MFB contractility with thrombin on θ (left panel) and dV/dt_{max} (right panel) in CMC and CMC-MFB cell strands.

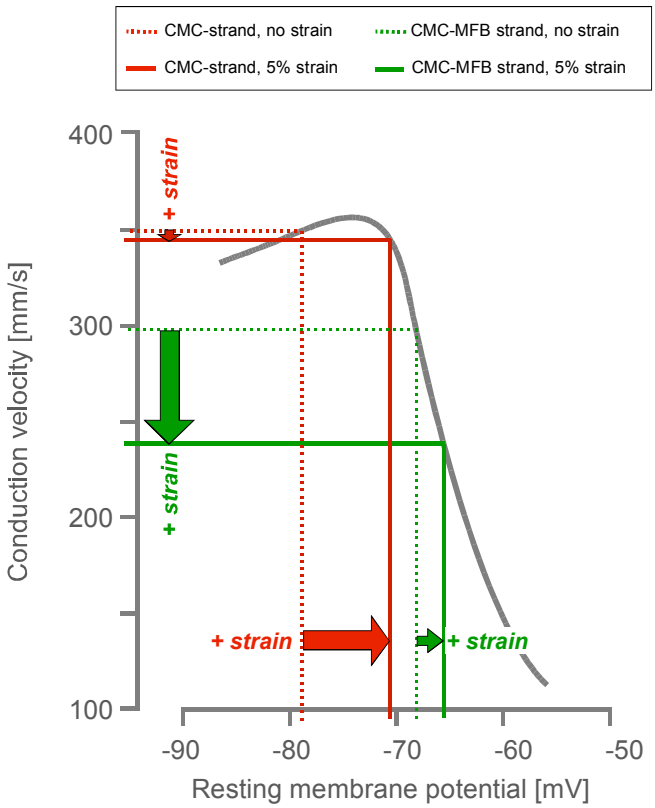

Figure 8

Figure 8 Schematic drawing illustrating the differential contributions of strain to conduction velocities in control CMC cell strands and in the fibrotic strand model consisting of CMC cell strands overlaid with MFBs. The grey curve indicates the dependence of θ measured in CMC cell strands on the resting membrane potential of CMCs ('supernormal conduction'; modified from[27]). The red lines refer to values obtained in CMC cell strands under non-strained control conditions (dashed) and during application of 5% strain (solid). A substantial stretch-induced depolarization of CMCs (horizontal red arrow) causes a modest change in conduction velocity (vertical red arrow). The green lines refer to values obtained in CMC-MFB cell strands (dashed = non-strained; solid = 5% strain). In these preparations, a modest stretch-induced depolarization (horizontal green arrow) causes a substantial change in conduction velocity (vertical green arrow).

SUPPLEMENT MATERIAL

Detailed Methods

Cell culture:

Primary cultures of neonatal rat ventricular cardiomyocytes (CMCs) and myofibroblasts (MFBs) were obtained using previously published methods.[1] Procedures used complied with relevant institutional guidelines for animal experimentation and were approved by the State Veterinary Department. In short, the apical two thirds of neonatal rat ventricles of 1-d old rats (Wistar) were cut into small pieces and dissociated in Hank's balanced salt solution (HBSS without Ca^{2+} and Mg^{2+}; Bioconcept) containing trypsin (0.1 %, Sigma) and pancreatin (120 µg/ml, Sigma). Complete tissue dispersion took 4 to 5 dissociation cycles lasting 15 min each. The dispersed cells were centrifuged and re-suspended in culture medium consisting of M199 with Hanks' salts (Sigma), penicillin (20'000 U/L; Sigma), vitamin B12 (1.5 µmol/L; Sigma) and 10% neonatal calf serum (Biochrom). Streptomycin was omitted from the cell culture media because it proved to interfere with the capacity of this drug to block mechanosensitive channels. The cell suspension was preplated for 2.2 h in cell culture flasks in order to separate fast adhering fibroblasts from slowly adhering CMCs. Non-adhering CMCs were pooled, passed through a cell strainer and vitamin C (18 µmol/L; Sigma), epinephrine (10 µmol/L; Sigma) and bromodeoxyuridine (100 µmol/L; Sigma) were added to the culture medium. Medium exchanges were performed every other day with supplemented M199 containing 5% neonatal calf serum. Fibroblasts obtained by the preplating procedure expressed α-smooth muscle actin within 24 to 48 hrs indicating their phenotype switch to MFBs.[2] MFBs were kept in culture for 8 days without passaging before being used in the experiments.

Single cell cultures: For patch clamp experiments, CMCs or MFBs were seeded on collagen (Type I or Type IV, Sigma) coated glass coverslips or on flexible substrates at 40 to 500 cells/ mm^2. Flexible substrates were made of silicone membranes measuring 0.25 x 30 x 50 mm (Silastic, SMI, USA). Membranes were activated with UV light (UVO Cleaner 342, Jelight, USA) for 8 min before being mounted on a digital caliper. After applying a pre-stretch of ~ 20%, a silicone ring (28/2 mm; Semadeni, Switzerland) was glued to the membrane with silicone adhesive (Elastosil E43, Wacher, Germany). This resulted in wells suitable for cell culture that were UV-sterilized before cell seeding.

Patterned growth cultures: For optical recordings of impulse propagation characteristics under non-strained control conditions, CMCs were seeded at a density of 1500 cells/mm^2 on photolithographically pretreated coverslips that were designed to produce uniform cell strands measuring 0.6 mm x 5 mm.[1] For strain experiments, pre-stretched flexible culture wells as described

above were used with the exception that following activation of the silicone membranes with UV light, lines of collagen were applied with a fine point nib to produce strands of CMCs. For the generation of hybrid CMC-MFB cell strands, cultured MFBs were dissociated using trypsin-containing solution (identical composition as that used for dissociation of cardiac tissue). Dispersed cells were collected, counted and seeded at a density of 500 cells/mm^2 on 24 h old patterned CMC preparations. After 2 h, cultures were washed with supplemented culture medium in order to remove non-adherent cells. Culture media composition was the same as that used for pure CMC cultures except that bromodeoxyuridine was omitted.

Optical measurement of action potential propagation:

Impulse propagation along strand preparations was assessed optically after staining the preparations for 4-5 min with the voltage sensitive dye di-8-ANEPPS (135 µmol/L; Biotium). Stained preparations were mounted in a temperature controlled chamber placed on the stage of an optical recording system described in detail elsewhere.[3] Preparations were superfused at a rate of 2-3 ml with HBSS at 36°C. Individual cell strands were stimulated with a bipolar electrode consisting of a glass micropipette filled with superfusion solution and a silver wire coiled around the shank. The electrode was placed ≥ 1 mm from measurement site in order to permit propagation to reach steady-state conditions at the recording site. Individual strands were pre-stimulated for 10s by a stimulator (SD9, Grass Instruments Co., Quincy, MA) at a basic cycle length of 500 ms before recording a single propagating action potential at a spatial resolution of 50 µm (20x magnification; Fluar 20x, 0.75 N.A., Zeiss, Switzerland). Signals were recorded at an analog bandwidth of 3 kHz and digitally filtered (f_o: 0.5 kHz) prior to analysis. Optically recorded action potential amplitudes were normalized (%APA) and maximal upstroke velocities (dV/dt_{max}) were calculated in units of %APA/ms. Under the assumption of an average APA of 100 mV, %APA/ms corresponds to V/s. Conduction velocities were derived from a linear fit of local activation times (time of 50% depolarization) along the preparation.[3] Only preparations exhibiting uniform conduction as indicated by linear fits exhibiting an $R^2 > 0.99$ were included in the analysis. Experimental data were obtained from 3-6 different cultures (4-8 different preparations each).

Patch-clamp recording:

Electrophysiological parameters of CMCs and MFBs were measured using a HEKA patch clamp system (EPC-10 amplifier, HEKA) controlled by PatchMaster software. Signals were filtered (1 kHz), digitized (2.9 kHz) and stored for off-line analysis with PatchMaster or FitMaster software (HEKA). The pipette filling solution contained (in mmol/L): K-aspartate 120, NaCl 10, MgATP 3, $CaCl_2$ 1, EGTA 10, Hepes 5 (pH 7.2). Pipette resistances ranged from 4 to 6 MΩ and pipette potentials were

zeroed before cell contact. Series resistance was compensated and voltage values were corrected for liquid junction potentials (- 12.4 mV) as calculated by pCLAMP software (Axon Instruments). Measurements were performed with cultures that were mounted in a custom-made chamber. Preparations were superfused at room temperature with HBSS at 2-3 ml/min. After seal formation (2-10 GΩ) and rupturing of the patch, cell capacity was compensated and the input resistance was calculated from voltage changes in response to a 5 pA hyperpolarizing current step. Resting membrane potentials were recorded in current clamp mode. Voltage clamp experiments using ramp protocols were applied to measure net membrane currents in single CMCs or MFBs. I-V relationships of CMCs were obtained by clamping the cells from – 80 to + 50 mV for 2 s before ramping the potential from +50 to -110 mV within 10 s. I-V relationships of MFBs were obtained from voltage ramps from -110 to 50 mV (1.6 s, starting from a holding potential of -70 mV). Whole cell currents were normalized to cell capacitance and are reported as pA/pF. For stretch/relaxation experiments, recordings were obtained 5 to 25 min after application of strain. Data were obtained from 3-6 different cultures (4-9 different preparations) for each experimental condition.

Quantification of strain experiments:

The stretch/relaxation induced deformation of flexible culture wells was quantified by marking the bottom with a triangular lattice of markers (n=16, spacing: 4 mm, forming 18 triangles). A digital photograph of the lattice (Canon EOS 1000D, 100 mm macro objective oriented perpendicular to the membrane) was taken before and after stretch. The photographs were corrected for geometric distortion (Adobe Photoshop CS5) using the corresponding lens correction data of the manufacturer and processed using custom software written in MatLab (The MathWorks, Natick, MA). The markers were identified semi-automatically, and, for each triangle, the deformation gradient tensor F was computed from the vertex coordinates. Strain (S) was then quantified based on the two eigenvalues (λ) of F and expressed in percent as $S=100\cdot(\lambda-1)$. The largest eigenvalue and the associated eigenvector ($\lambda>1$, $S>0$) correspond to stretch along the caliper axis. Measurements using this procedure confirmed that stretch was uniform within the silicone ring (maximal deviation: 2.4% of overall stretch applied) and that the deviation of the main stretch axis from the caliper axis was less than 1 degree. The smallest eigenvalue, typically <1, corresponds to a concomitant shortening ($S<0$) in the perpendicular direction. Because the membrane was not stabilized in the transverse direction, longitudinal stretch was accompanied by transverse stricture.

Wrinkle experiments:

Substrates for the wrinkle assay (coverslips with a thin coat of soft polymer, Excellness, Switzerland) were coated with collagen type IV and sterilized with UV. Myofibroblasts seeded at low density (100 cells/mm^2) produced prominent wrinkles of the substrate within 1-2 days. Preparations were mounted in a temperature-controlled experimental chamber that was placed on the stage of an inverted microscope and wrinkle formation was followed by a high resolution camera under phase contrast illumination. Cells were continuously superfused at 36°C with standard HBSS solution. Time lapse video recordings were started after a stabilization period of approx. 4 min and continued for 30 min after addition of blebbistatin (10 µmol/L) or thrombin (1 U/mL) to the superfusate. Custom-made software (MatLab with Imaging Processing Toolbox; The MathWorks, Natick, MA) was used to quantify the time course of change of the wrinkle area during the experiment. The algorithm used served to detect the typical features of wrinkles as observed under phase contrast illumination which consist of long-oval shaped regions being either bright or dark due to the formation of valleys and crests. To isolate regions with these features, phase contrast images were first subjected to simultaneous low-brightness ('valleys') and high-brightness ('crests') thresholding before undergoing feature extraction accounting for the typical long-oval shapes. Including minimal size requirements prevented false positive detection of small oval shaped objects as produced, e.g., by cell debris. For movies, the interval of images to be analyzed was user-selectable. Results were checked by eye for correctness before automatic generation of an excel table containing the relevant data.

Immunocytochemistry

Preparations grown on silicone membranes remained fixed to the digital caliper and were washed with phosphate buffered saline (PBS, Invitrogen) followed by fixation with 2% paraformaldehyde at room temperature (RT) for 5 min. Thereafter, they were incubated for 20 min with blocking buffer (PBS containing 20% goat serum) before being exposed for 2 h to anti-α-smooth muscle actin (mouse monoclonal, Thermo Fisher) dissolved in PBS containing 1% goat serum and 0.15% triton X-100. After washing, preparations were incubated for 20 min at RT with secondary antibodies (Alexa Fluor 488 goat anti-mouse, Molecular Probes) containing DAPI (Molecular Probes). After washing, the preparations remaining submersed in buffer were immediately imaged on an inverted microscope equipped for epifluorescence (Zeiss, Axiovert 200) using a slow-scan camera (Spot RT, Diagnostic Instruments).

Similar protocols were used to investigate expression of mechanosensitive channels in low density cultures of cardiac myofibroblasts. Preparations were incubated with primary antibodies against

TRPC6 (guinea pig, polyclonal), TRPM4, TRPM7 and TRPV2 (rabbit, polyclonal; all antibodies from Alomone) followed by incubation with secondary antibodies (Cy3, goat anti-guinea pig; Chemicon; Alexa Fluor 546, goat anti-rabbit, Molecular Probes) containing DAPI (Molecular Probes). Primary antibodies pre-incubated with the respective control peptides served as control. After a final wash step, preparations were mounted in Fluoroshield (ImmunoBioScience) and imaged using the same setup as described above. Illumination parameters and brightness adjustments between experimental preparations and control preparations are identical.

Solutions and drugs:

In all experiments, preparations were superfused at 2-3 ml/min with Hank's balanced salt solution (AppliChem) containing 1% neonatal calf serum and (mmol/L) NaCl 137, KCl 5.4, $CaCl_2$ 1.3, $MgSO_4$ 1.2, $NaHCO_3$ 4, KH_2PO_4 0.5, NaH_2PO_4 0.3, Glucose 5.5 and HEPES 10 titrated to pH 7.40 with 1 mol/L NaOH. For gadolinium experiments, preparations were superfused with solution devoid of phosphate and bicarbonate that contained (in mmol/L): NaCl 140, KCl 5.4, $CaCl_2$ 1.8, $MgCl_2$ 1.2, Glucose 20, Hepes 5 (pH 7.40).[4] Drugs used were obtained from Sigma with the exception of thrombin (Biopur AG, Switzerland).

Expanded Results and Discussion

Time course of change in wrinkle area following addition of blebbistatin (movie 1)

The time-lapse movie (6 frames/min) illustrates the blebbistatin-induced change of the wrinkle pattern produced by the tensile forces of a single myofibroblast on the soft polymer substrate (same experiment as that depicted in Figure 6A of the manuscript). The data window below the phase contrast movie indicates the decrease in wrinkle area following addition of 10 μmol/L blebbistatin to the superfusate (round progress indicator switches color from black to red after addition of the drug). The first part of the movie shows the raw video sequence whereas the second part shows the computed wrinkle area (red to white) overlaid on the raw video.

Average normalized data describing the time course of change in wrinkle area following addition of 1 U/ml thrombin and 10 μmol/L blebbistatin to myofibroblasts cultured on soft polymer substrates are shown in Figure 1. Data were normalized to the mean wrinkle area recorded during the first 4 minutes (control) and the last 4 minutes of the exposure to drugs. Half-maximal effects of thrombin were reached after ~ 2 min whereas, for blebbistatin, half-maximal effects were seen after ~ 7 minutes.

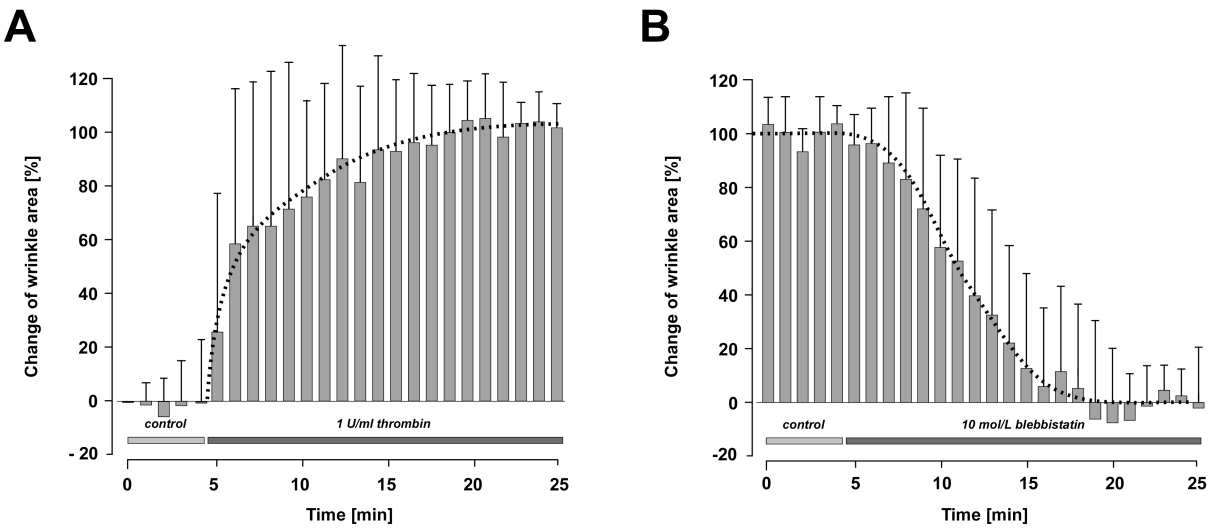

Figure 1: Time course of change in wrinkle area following stimulation/suppression of tension developed by myofibroblasts (normalized). **A**: Time course of changes in wrinkle area following addition of 1 U/ml thrombin (average + SD; n= 10). **B**: Time course of changes in wrinkle area following addition of 10 µmol/L blebbistatin (average + SD; n= 9). Fits (dashed lines) drawn by hand.

I-V relationship of cardiac myofibroblasts stretched by 10%

To characterize transmembrane currents of myofibroblasts at increased levels of mechanical stress, we raised the longitudinal strain to 10% in a subset of patch clamp experiments. The data shown in Figure 2 below illustrate that this intervention caused a marked accentuation of mechanosensitive currents when compared to currents elicited by 5 % strain (data from Figure 4A in the manuscript). Mechanosensitive currents elicited by 10% strain showed a nearly linear I-V relationship with a reversal potential at –10 mV. Attempts to investigate the consequences of this additional current on conduction in CMC-MFB cell strands failed because, unlike CMC-only cell strands, these hybrid preparations tended to detach when stretched by 10%.

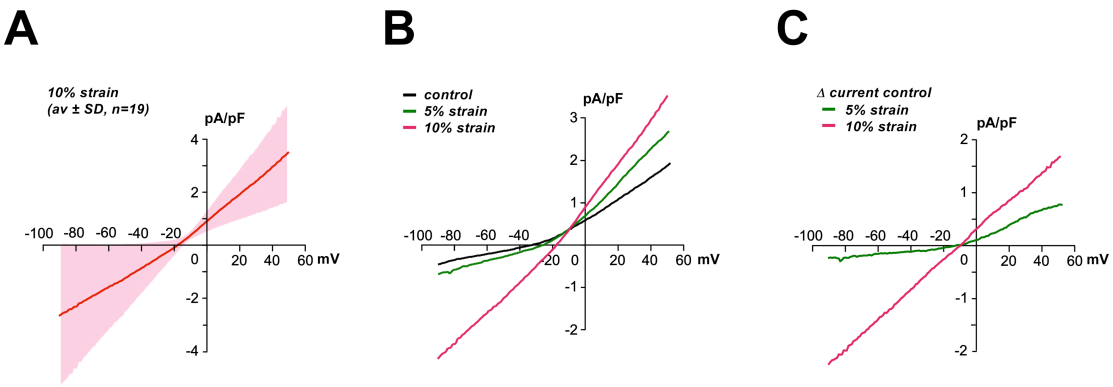

Figure 2: Comparison of IV-relationships recorded in myofibroblasts at 0% (control), 5% and 10% strain. **A**: IV-relationship of myofibroblasts strained by 10% (average ± SD; n= 13). **B**: Comparison of average currents recorded in myofibroblasts under control conditions (black, data from manuscript), during 5% strain (green, data from manuscript) and during 10% strain. **C**: Difference currents vs. control recordings for 5% strain (green) and 10% strain (red).

Expression of mechanosensitive channels in cultured cardiac myofibroblasts

A previous qPCR screen indicated substantial expression of the mechanosensitive channels TRPC6, TRPM4, TRPM7 and TRPV2 at the RNA message level in cultured cardiac myofibroblasts.[5] Using immunocytochemistry, we now found that TRPV2 and TRPC6 are expressed and associated with the cell membrane of cardiac myofibroblasts. As shown in Figure 3, TRPV2 shows a distinct labeling of the leading lamella of myofibroblasts whereas TRPC6 is primarily targeted to regions of cell-to-cell apposition. Given that expression of TRPV2 has previously been associated with the migratory behavior of cancer cells,[6] its enhanced expression at the leading lamella may point to a similar function in cardiac myofibroblasts. On the other hand, the functional consequences of the novel observation of a distinct targeting of TRPC6 to sites of cell-to-cell are still unclear. In contrast to the distinct labeling observed for TRPV2 and TRPC6, antibodies against TRPM4 and TRPM7 failed to produce a signal clearly different from control preparations (data not shown).

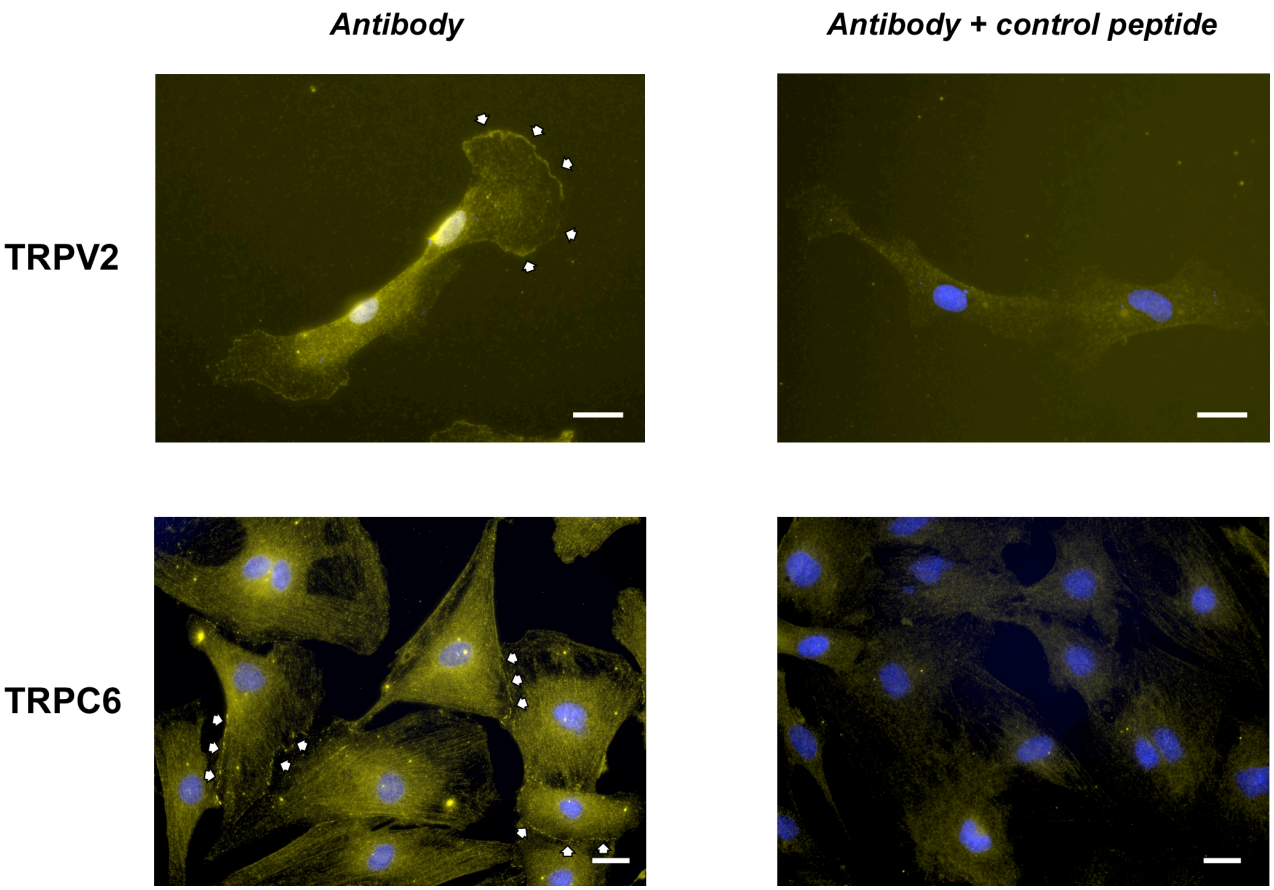

Figure 3: Immunofluorescence detection of mechanosensitive ion channels in cardiac myofibroblasts. TRPV2 (upper row): Apart from cytoplasmic and nuclear expression, TRPV2 (yellow) is targeted to the leading lamella (white arrows). Nuclei are counterstained with DAPI (blue). TRPC6 (lower row): TRPC6 is present in the cytoplasm and targeted to sites of cell-to-cell contact (white arrows). Scale bars: 20 µm.

References:

1. Rohr S, Flueckiger-Labrada R, Kucera JP. Photolithographically defined deposition of attachment factors as a versatile method for patterning the growth of different cell types in culture. *Pflugers Arch* 2003;**446**:125-132.
2. Rohr S. Cardiac fibroblasts in cell culture systems: myofibroblasts all along? *J Cardiovasc Pharmacol* 2011;**57**:389-399.
3. Rohr S, Kucera JP. Optical recording system based on a fiber optic image conduit: assessment of microscopic activation patterns in cardiac tissue. *Biophys J* 1998;**75**:1062-1075.
4. Kamkin A, Kiseleva I, Isenberg G. Activation and inactivation of a non-selective cation conductance by local mechanical deformation of acutely isolated cardiac fibroblasts. *Cardiovasc Res* 2003;**57**:793-803.
5. Rosker C, Salvarani N, Schmutz S, Grand T, Rohr S. Abolishing myofibroblast arrhythmogeneicity by pharmacological ablation of alpha-smooth muscle actin containing stress fibers. *Circ Res* 2011;**109**:1120-1131.
6. Monet M, Lehen'kyi V, Gackiere F, Firlej V, Vandenberghe M, Roudbaraki M, Gkika D, Pourtier A, Bidaux G, Slomianny C, Delcourt P, Rassendren F, Bergerat JP, Ceraline J, Cabon F, Humez S, Prevarskaya N. Role of cationic channel TRPV2 in promoting prostate cancer migration and progression to androgen resistance. *Cancer Res* 2010;**70**:1225-1235.